ORIGINAL ARTICLE

Dynamic ^{18}F-FDG PET for Assessment of Tumor Physiology in Two Breast Carcinoma Xenografts

**Alexandr Kristian · Line B. Nilsen · Kathrine Røe · Mona-Elisabeth Revheim ·
Olav Engebråten · Gunhild M. Mælandsmo · Ruth Holm ·
Eirik Malinen · Therese Seierstad**

Abstract

Purpose To compare dynamic 2-deoxy-2-[^{18}F]fluoro-D-glucose positron emission tomography (^{18}F-FDG PET) parameters in two selected human breast cancer xenografts and to evaluate associations with immunohistochemistry and histology.

Procedures Dynamic ^{18}F-FDG PET of luminal-like MAS98.06 and basal-like MAS98.12 xenografts was performed, and the compartmental transfer rates (k_1, k_2, k_3), blood volume fraction (v_B) and metabolic rate of ^{18}F-FDG(MR_{FDG}) were estimated from pharmacokinetic model analysis. After sacrifice, analyses of hypoxia (pimonidazole), proliferation (Ki-67), vascularization (CD31), glucose transport receptor (GLUT1) and necrosis (HE) was performed. The level of hexokinase 2 (HK2) was estimated from Western blot analysis.

Results The ^{18}F-FDG uptake curves for the two xenografts were significantly different ($p<0.05$). k_1 and v_B were higher for MAS98.12 ($p<0.01$), while k_3 was higher for MAS98.06 ($p<0.01$). MAS98.12 had a higher fraction of stromal tissue and higher microvessel density (MVD), and it was less necrotic and hypoxic than MAS98.06. MAS98.12 had stronger positive GLUT1 staining and lower Ki-67 than MAS98.06. In both models significant correlations were found between k_1 and the GLUT1 score, between k_3 and the level of HK2, and between v_B and MVD.

Conclusions Significant differences in dynamic ^{18}F-FDG parameters between the two human breast cancer xenografts were found. The differences could be explained by underlying histological and physiological characteristics.

Keywords Dynamic ^{18}F-FDG PET · Kinetic analysis · Breast carcinoma · GLUT1 · Ki-67 · Perfusion

Introduction

Individualized cancer treatment in clinical practice requires knowledge of the underlying tumor physiology, determining the tumor aggressiveness and the anticipated therapeutic

A. Kristian · O. Engebråten · G. M. Mælandsmo
Department of Tumor Biology, Institute for Cancer Research,
Oslo University Hospital, 0424 Oslo, Norway

L. B. Nilsen · K. Røe
Department of Radiation Biology, Institute for Cancer Research,
Oslo University Hospital, 0424 Oslo, Norway

A. Kristian · L. B. Nilsen · K. Røe · M.-E. Revheim
Institute of Clinical Medicine, University of Oslo, 0316
Oslo, Norway

M.-E. Revheim · T. Seierstad (✉)
Department of Radiology and Nuclear Medicine,
Oslo University Hospital, 0424 Oslo, Norway
e-mail: therese.seierstad@ous-hf.no

O. Engebråten
Department of Oncology, Oslo University Hospital, 0424
Oslo, Norway

G. M. Mælandsmo
Department of Pharmacy, Faculty of Health Sciences,
University of Tromsø, 9037 Tromsø, Norway

R. Holm
Department of Pathology, Oslo University Hospital, 0424
Oslo, Norway

E. Malinen
Department of Medical Physics, Oslo University Hospital, 0424
Oslo, Norway

E. Malinen
Department of Physics, University of Oslo, 0316 Oslo, Norway

T. Seierstad
Department of Health Sciences, Buskerud University College,
3007 Drammen, Norway

response. Factors known to influence therapeutic outcome are, among others, tumor cell proliferation, vascularization and tumor hypoxia [1, 2]. Tumors are heterogeneous with respect to these factors, and biopsies may thus not be representative for the entire tumor. Medical imaging techniques may provide information on the biology and functionality of the entire lesion. Such assessment of heterogeneous tumor characteristics may enable more biologically adapted, individualized treatment regimens.

Breast cancer is one of the most common cancer types in women [3]. The disease is characterized by biological heterogeneous features, with a lack of reliable biomarkers to guide therapy selection, making the clinical management challenging [4]. Based on gene expression profiles, five molecular subtypes of breast cancer have been determined [5, 6]. These gene expression profiles have been shown to define subgroups of patients with different outcomes [7], signifying that the subgroups have special treatment requirements.

Conventional 2-deoxy-2-[^{18}F]fluoro-D-glucose (^{18}F-FDG) positron emission tomography (PET) for cancer imaging exploits the accumulation of ^{18}F-FDG in cancer cells with high glucose demand [8]. The conventional, clinical assessment of ^{18}F-FDG uptake is based on the standardized uptake value (SUV) calculated from static ^{18}F-FDG PET images acquired typically 1 h post injection. Since SUV is subjected to many sources of variability, which often are not controlled or accounted for (e.g., body composition and habitus, duration of the uptake period, plasma glucose levels, recovery coefficients and partial volume effects [9]), its interpretation may potentially be misleading. Despite its limitations, changes in SUV can be predictive for treatment outcome [9]. In contrast to conventional ^{18}F-FDG PET, dynamic ^{18}F-FDG PET depicts the distribution of ^{18}F-FDG in space and time from the time of injection, thus reflecting both the early tissue distribution phase and the later metabolic phase [10]. Pharmacokinetic modeling of the tracer uptake can provide information beyond SUV, for example, on blood flow and tumor metabolism [11]. Reliable non-invasive depiction of the tumor microenvironment is likely to improve assessment of tumor aggressiveness and prediction of treatment outcome [12]. A prerequisite for clinical use of dynamic ^{18}F-FDG PET for imaging tumor physiology is knowledge on how imaging parameters relate to underlying tumor microenvironmental features. In this study, we explore such associations in two xenografts representing different genetic breast cancer subclasses with anticipated differences in prognosis [5, 13].

Materials and Methods

Animals and Xenografts

Eleven female athymic nude mice (Athymic Nude-Foxn1^{nu}; weight, 23–25 g; age, 11–13 weeks) bearing bilateral human breast MAS98.12 ($n=11$) or MAS98.06 ($n=10$) xenografts were used. Both the estrogen- and progesterone-receptor-positive MAS98.06 and the triple-negative MAS98.12 were pathologically characterized as invasive ductal carcinoma grade III [13]. Molecular characterization of the two xenografts has classified MAS98.06 and MAS98.12 as luminal- and basal-like subtype, respectively. The protocol was approved by The National Animal Research Authority, and the experiment was conducted according to the regulations of the Federation of European Laboratory Animal Science Association (FELASA).

Mice were bred at the institutional Department of Comparative Medicine and kept under pathogen-free conditions, at constant temperature (21.5±0.5 °C) and humidity (55±5 %), 20 air changes/h and a 12 h light/dark cycle. Distilled tap water was given ad libitum, supplemented with 17-β-estradiol at a concentration of 4 mg/l to ensure growth in the estrogen-dependent MAS98.06 xenografts.

Tumor tissue fragments measuring $2 \times 2 \times 2$ mm^3, obtained from a previous passage, were implanted bilaterally in the mammary fat pads. When the longest tumor diameter was between 8 and 10 mm, 4 to 8 weeks after implantation, respectively, for MAS98.12 and MAS98.06, mice were subjected to dynamic ^{18}F-FDG PET (see below).

Collection and use of biopsies from primary breast cancer patients for establishment of xenografts in immunodeficient mice were approved by the South-East National Committee for Medical and Health Research Ethics (approval no. S-07398a).

Anesthesia

Prior to implantation of xenografts and ^{18}F-FDG PET, mice were anesthetized with subcutaneous (s.c.) injections of a mixture of 2.4 mg/ml tiletamine and 2.4 mg/ml zolazepam (Zoletil vet, Virbac Laboratories, Carros, France), 3.8 mg/ml xylazine (Narcoxyl vet, Roche, Basel, Switzerland) and 0.1 mg/ml butorphanol (Torbugesic, Fort Dodge Laboratories, Fort Dodge, IA), diluted 1:5 in sterile water, at a dosage of 75 μl/10 g of body weight.

PET Imaging

Dynamic ^{18}F-FDG PET was performed using a Siemens microPET Focus 120 (Erlangen, Germany) animal scanner. Following overnight fasting, the animals were anesthetized and a catheter flushed with heparinized saline was inserted in the tail vein. Groups of 2–3 mice were placed on the examination table, centered within the scanner gantry. A 50-min PET acquisition in list mode was started prior to i.v. administration of 5–10 MBq ^{18}F-FDG (GE Healthcare AS, Oslo, Norway) diluted in heparinized saline. Attenuation and scatter correction was obtained by acquiring a 10-min transmission scan with a ^{68}Ge point source. The 3D dynamic emission data

were reconstructed using OSEM-MAP (2 OSEM iterations, 18 MAP iterations, β=0.5, matrix size=128×128×95) [14], producing images with voxel size 0.87×0.87×0.80 mm^3. The sampling time ranged from 15 s (early time points) to 600 s (late time points).

All images were saved in the DICOM format and transferred to a remote PC for post-processing and kinetic modeling using in-house-written IDL programs (Interactive Data Langue, v6.2, Research Systems Inc., Boulder, CO).

Quantitative Evaluation and Kinetic Modeling of Dynamic ^{18}F-FDG PET

Individual arterial input functions (AIFs) were obtained by fitting the ^{18}F-FDG time activity curve (TAC) from the left ventricle to a bi-exponential function using Levenberg-Marquardt least squares minimization, as described by Røe et al. [15].

Tumor tissue was manually delineated in the axial PET images, and TACs for individual tumors were obtained. TACs were normalized to the AIF, thus accounting for differences in injected ^{18}F-FDG activity between animals [15].

The ^{18}F-FDG TAC from each voxel was subjected to kinetic modeling using a two-compartment model, described in detail elsewhere [15]. Briefly, the model assumes that the tracer concentration in the tissue, C_T, can be separated in a free (non-metabolized) and a bound (metabolized) compartment, with tracer concentrations C_F and C_B, respectively. The four rate constants in the model, k_1, k_2, k_3 and k_4, describe the exchange of ^{18}F-FDG between the two compartments. The kinetic parameters are estimated by non-linear least squares fitting of the model to the TAC. k_4 was assumed to be low and set to zero in the calculations. The blood volume fraction, v_B, was estimated as described by Kamasak et al. [16]. The metabolic rate of ^{18}F-FDG, MR_{FDG}, was calculated as $(k_1 k_3)/(k_2+k_3)$. The goodness of fit between the measured TACs and the model fits was evaluated by Pearson's correlation coefficient squared (r^2) in each tumor voxel. The median kinetic parameter value over the voxels in each tumor was calculated and used.

Histology and Immunohistochemistry

To assess tumor hypoxia and functional vasculature, mice received 0.5 ml i.p. injections of pimonidazole hydrochloride (80 mg/kg, 1-[(2-hydroxy-3-piperidinyl)propyl]-2-nitroimidazole hydrochloride; Natural Pharmaceuticals, International Inc., Research, Triangle Park, NC, USA) and 0.1 ml i.v. injection of Hoechst 33342 (15 mg/kg, Sigma Chemical Co, St Louis, MO, USA), 1 h and 5 min, respectively, prior to being killed by neck dislocation. To match the in vivo imaging slices, the xenografts were excised and divided in two along the axial plane. One half was snap-frozen in liquid nitrogen

and stored at −80 °C, while the second half was formalin-fixed and paraffin-embedded.

Assessment of hypoxia, necrosis, proliferation (Ki-67), expression of glucose transporter 1 (GLUT1) and vascularization (CD31) was performed on consecutive 5-μm sections from paraffin blocks. Sections from paraffin blocks were deparaffinized and rehydrated in graded alcohols for hematoxylin and eosin (HE) staining and immunohistochemical staining for Ki-67, GLUT1, CD31 and pimonidazole.

After incubation with monoclonal antibody against Ki-67 (clone Ki-S5, 1:100, Dako, Glostrup, Denmark), polyclonal antiserum against GLUT1 (1:200, Abcam, Cambridge, UK) or CD31 (1:50, Abcam, Cambridge, UK) for 30 min, the sections were treated with peroxidase-labeled polymer conjugated to goat anti-mouse IgG or goat anti-rabbit IgG (EnVision+kit, Dako, Glostrup, Denmark) for 30 min. Tissue sections were stained for 10 min with 3′3-diaminobenzidine tetrahydrochloride (DAB) and counterstained with hematoxylin, dehydrated and mounted in Diatex (Becker Industrifarg, Marsta, Sweden). All series included positive controls. Negative controls included substitution of (1) monoclonal antibody with mouse myeloma protein of the same subclass and concentration as the monoclonal antibody and (2) substitution of the polyclonal antiserum with normal rabbit serum of the same dilution as the polyclonal antiserum. Only nuclear staining for Ki-67 and membrane staining for GLUT1 were considered positive.

Semiquantitative classes were used to describe the intensity (absent, 0; weak, 1; moderate, 2; strong, 3) and the extent of Ki-67 and GLUT1 staining (percentage of positive tumor cells: absent, 0; <10 %, 1; 10–50 %, 2; 51–75 %, 3; >75 %, 4). By multiplying the intensity with the extent of staining, scores ranging from 0 to 12 were obtained.

The pimonidazole-labeled cells were detected by a peroxidase-based immunohistochemical assay using affinity purified rabbit anti-pimonidazole antibody (PAb2627AP) and goat anti-rabbit IgG (EnVision+Kit, Dako, Glostrup, Denmark) as previously described [17].

Section imaging was performed using a CellObserver microscope system (Carl Zeiss Microimaging GmbH, Göttingen, Germany) equipped with an EC PlanNeofluar 10x/0.3 Phase 1 lens, a LD condenser 0.55H, a Definite Focus system, a motorized high resolution scanning stage and an AxioCam MRm camera. Initial image processing (single images stitching and correction of white balance) was performed using AxioVision software (Carl Zeiss Microimaging GmbH, Göttingen, Germany). Areas of hypoxia and necrosis were determined by visual inspection and manual delineation using ImageJ (NIH, MA, USA). Regions showing pimonidazole staining were scored as positive, irrespective of signal staining intensity. The fractions were determined relative to the total tumor area. The number of vessels was counted in the whole section, and microvessel

density (MVD) was determined as MVD=(number of vessels)/(total area of the section in mm^2).

Western Blot Analysis

Immunoblotting was used to measure the levels of HK2 in the two xenografts. Protein lysate from 25–40-μm sections of snap-frozen tissue was prepared using M-PER mammalian protein extraction reagent containing halt protease and phosphatase inhibitors cocktail (both Thermo Fisher Scientific, IL, USA) according to a standard protocol. Protein concentration was determined by measuring absorption at 280 nm using a NanoDrop 2000c Spectrophotometer (Thermo Fisher Scientific, IL, USA). Proteins were separated using a sodium dodecyl sulfate polyacrylamide gel electrophoresis, transferred to a nitrocellulose membrane and probed with anti-HK 2 antibody (ab37593, dilution 1:100, Abcam, MA, USA), followed by a peroxidase-conjugated anti-rabbit secondary antibody (1:2000, Dako, Glostrup, Denmark). To control for the amount of loaded protein, β-actin was stained using monoclonal anti-β-actin mouse antibody (A5316, clone AC-74, 1:10000, Sigma, St Louis, MO, USA) and peroxidase-conjugated anti-mouse secondary antibody (1:5,000, Dako, Glostrup, Denmark). Visualization was performed using a SuperSignal West Dura Luminol/Enhancer solution (Pierce, Rockfold, IL).
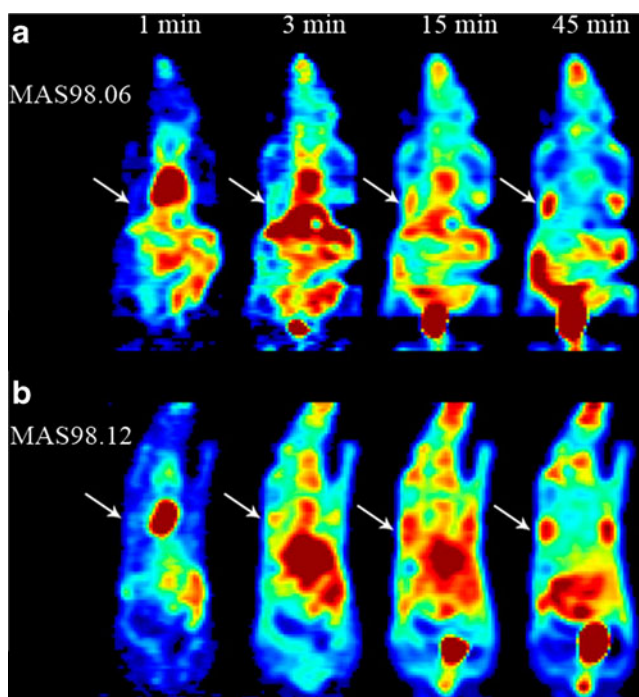
Membranes were exposed in the G:Box fluorescence imaging system (Syngene, Cambridge, UK) for 10 min to measure the intensity of HK2 bands. The HK2 level was determined by normalizing the intensity of HK2 bands to the intensity of the respective β-actin bands.

Statistics

Correlation between kinetic parameters and histologically assessed tumor characteristics were assessed using Pearson's correlation coefficient and the two-sided t-test. Kinetic parameters and histological features of MAS98.06 and MAS98.12 were compared using the Mann-Whitney U test in the IDL software. The statistical significance level was 0.05.
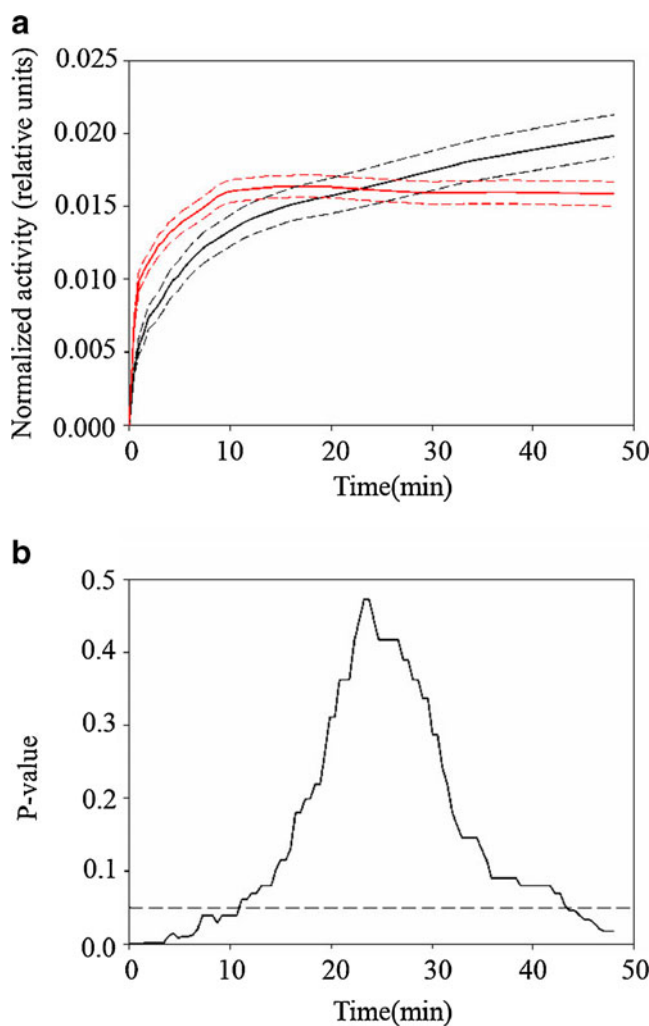

Fig. 2 Mean (solid lines) and standard deviation (dotted lines) of normalized time activity curves (TACs) for the two human breast cancer xenografts MAS98.06 (black) and MAS98.12 (red) (upper panel, a). Using Mann-Whitney U tests, significant differences between the two xenografts were found in the initial uptake phase and at the end of the examination (lower panel, b)

Fig. 1 Dynamic ^{18}F-FDG PET images of the human breast cancer xenografts MAS98.06 (a) and MAS98.12 (b), at 1, 3, 15 and 45 min after bolus injection. White arrows show the locations of the tumors

Fig. 3 ^{18}F-FDG uptake 50 min after bolus injection shows heterogeneity in trancer distribution within a selected region of interest (in black) for a human breast cancer xenograft MAS98.06 (**a**). Activity concentration as function of time, fitted curves and curves for free and bound components obtained from kinetic modeling from two selected voxels in the central (I) and peripheral zone (II) (**b**) shows a similar free component kinetic. The growth of the bounded component is faster in the voxel from the central zone. This is also reflected in the parametric maps for k_1, k_2, k_3 and MR_{FDG} (**c**) corresponding to the region of interest in (**a**). Values of k_1 and k_2 are spatially independent, whereas k_3 and MR_{FDG} are higher for the central than the peripheral zone
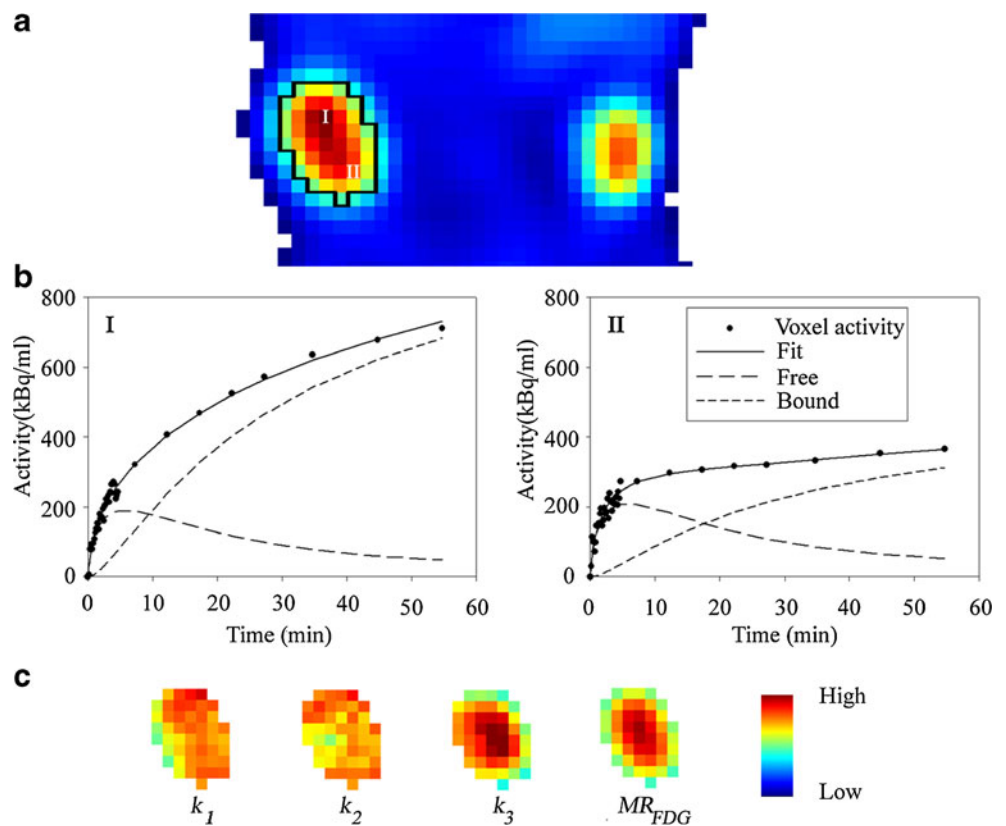
Results

Qualitative and Quantitative Assessment of PET Images

Figure 1 shows ^{18}F-FDG PET images at four different time intervals for two mice bearing MAS98.06 (a) or MAS98.12 (b) xenografts. For both xenografts, the ^{18}F-FDG concentration increased with time after injection. In Fig. 2a, the mean normalized TACs for the two groups of xenografts are shown. The MAS98.06 xenografts exhibited a slower initial uptake and did not reach a plateau during the examination period. In contrast, the MAS98.12 xenografts had a faster initial ^{18}F-FDG uptake, but the uptake reached a plateau around 10 min post injection. Normalized TACs were significantly different between the two xenografts in the time periods 0–12 min and 44–48 min (Fig. 2b).

^{18}F-FDG TACs and the results from pharmacokinetic modeling for a voxel in the central zone and for a voxel in the peripheral zone of a MAS98.06 xenograft are shown in Fig. 3a. In addition to the raw and fitted data, Fig. 3b also shows the free and bound components of ^{18}F-FDG derived from the fitting. Both voxels have a similar free component, whereas the bound component is more pronounced in the central voxel. The pharmacokinetic model analysis fits the PET data with high accuracy, regardless of the underlying uptake patterns. After pharmacokinetic model analyses of all tumor voxels, parametric maps were generated (Fig. 3c). For this particular MAS98.06 xenograft, the k_1 and k_2 maps were rather uniform, whereas k_3 and MR_{FDG} showed an increasing gradient towards the centre of the xenograft. The v_B maps were heterogeneous and less systematic, with large regions having little or no intensity (data not shown).

Table 1 Median and range of the rate constants k_1, k_2, k_3, MR_{FDG} and v_B in the human breast cancer xenografts MAS98.06 and MAS98.12. The two models were significantly different in the k1, k3 and vB parameters. The p-values were obtained from the Mann–Whitney U test

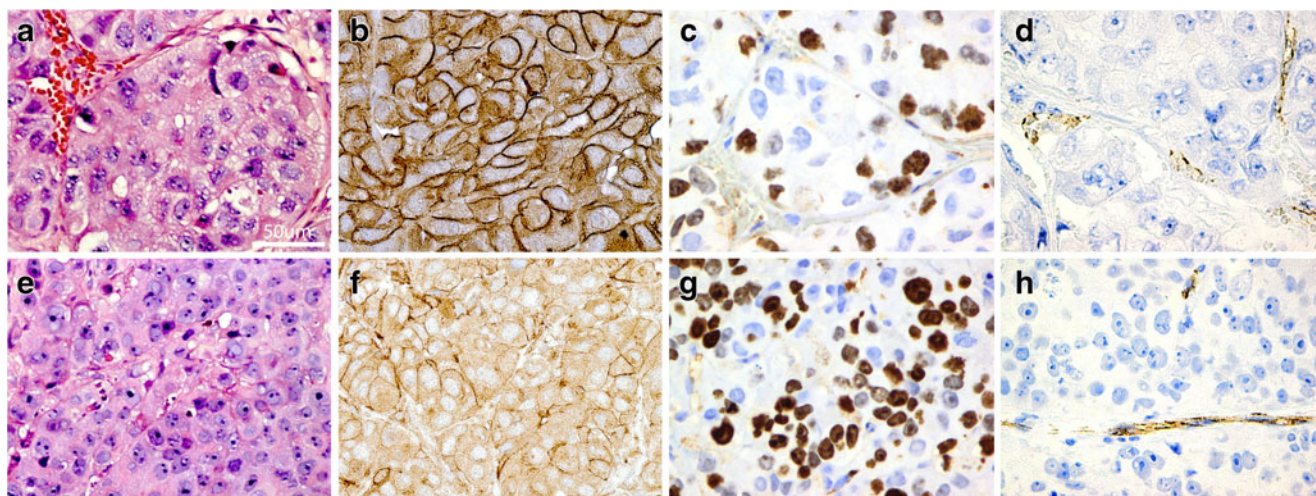|	MAS98.06	MAS98.12	P-value
k_1 (min^{-1})	0.086 (0.033, 0.127)	0.122 (0.094, 0.192)	<0.01
k_2 (min^{-1})	0.158 (0.068, 0.298)	0.185 (0.146, 0.296)	0.20
k_3 (min^{-1})	0.037 (0.019, 0.086)	0.011 (0.007, 0.024)	<0.01
MR_{FDG} (min^{-1})	0.010 (0.006, 0.025)	0.007 (0.004, 0.012)	0.09
v_B	0 (0.000, 0.032)	0.015 (0.000, 0.070)	<0.01

Fig. 4 Histological sections for the human breast cancer xenografts MAS98.12 (**a, b, c, d**) and MAS98.06 (**e, f, g, h**). Hematoxylin and eosin (a and e), membrane staining for GLUT1 (b and f), Ki-67 (c and g) and CD31 (d and h). Magnification 40×

The goodness of the pharmacokinetic model fit ranged from 0.94 to 0.99 and was not significantly different between the two groups (p=0.72). Median k_1, k_2, k_3, MR_{FDG} and v_B for both xenografts are summarized in Table 1. The influx k_1 parameter and blood volume fraction v_B were significantly higher for the MAS98.12 xenografts compared to the MAS98.06 xenografts. In contrast, k_3 was significantly higher for MAS98.06.

Immunohistochemical Analysis

Figure 4 shows immune staining with antibodies against GLUT1, CD31, Ki-67 as well as HE-stained sections for both xenografts. The HE stains showed that MAS98.12 contained more stromal tissue than MAS98.06, while the latter was more homogeneous. GLUT1 showed a stronger membrane staining in MAS98.12 compared to MAS98.06, and staining with CD31 revealed higher MVD in MAS98.12. Conversely, nuclear staining with Ki-67 was more prominent in MAS98.06. MAS98.12 xenografts generally exhibited less necrosis and hypoxia compared to MAS98.06 xenografts (histological sections not shown). The corresponding quantitative findings are summarized in Table 2. Scoring of GLUT1 revealed that MAS98.12 xenografts had a strong

positive membrane staining in more than 75 % of the cells, with a median score value of 12. In contrast, the MAS98.06 xenografts had weaker GLUT1 staining in a smaller fraction of the cells, resulting in a median score of 6. MVD was 1.2 fold higher in MAS98.12 xenografts than in MAS98.06 xenografts. The fraction of Ki-67 positive nuclei was above 75 % for MAS98.06 xenografts sections compared to 50–75 % for MAS98.12 (median scores of 12 and 9, respectively). Quantification of HK2 by Western blot analysis in MAS98.06 xenografts had 2.1 fold higher expression (p=0.030) than in MAS98.12 xenografts.

Correlation Kinetic Parameters and Histology

Correlations among the PET parameters (k_1, k_2, k_3, MR_{FDG} and v_B) and histologically assessed tumor characteristics are summarized in Table 3. Among others, the influx k_1 parameter was significantly positively correlated with GLUT1. Furthermore, metabolic parameters k_3 and MR_{FDG} showed significant positive correlation with Ki-67 and with the relative level of HK2. The blood volume fraction v_B correlated positively with MVD. Finally, no significant correlation with the necrotic or hypoxic fraction was found for either of the kinetic parameters.

Table 2 Median and range of histological parameters in the human breast cancer xenografts MAS98.06 and MAS98.12. The differences in the respective parameters between the two models were tested using the Mann–Whitney U test

	MAS98.06	MAS98.12	P-Value
Necrotic fraction, %	8.7 (0.8, 20.6)	0.0 (0.0, 20.7)	0.05
Hypoxic fraction, %	37.8 (14.9, 45.0)	16.9 (1.2, 52.7)	0.04
Microvessel density[*]	55.1 (36.6, 63.8)	66.0 (50.8, 100.6)	0.04
Relative level of HK2	0.45 (0.21, 0.61)	0.22 (0.13, 0.24)	0.03
Ki-67 Score	12 (12)	9 (6–12)	< 0.01
GLUT1 Score	6 (6, 9)	12 (12)	< 0.01

[*] In vessels/mm^2

Table 3 Pearson's correlation coefficients between the rate constants k_1, k_2, k_3, MR_{FDG} and v_B and histological assessed tumor characteristics. Values from both breast cancer xenograft models were utilized, and the p-values (in parentheses) were obtained using two-sided t-tests

	k_1 (min^{-1})	k_2 (min^{-1})	k_3 (min^{-1})	MR_{FDG} (min^{-1})	v_B
Necrotic fraction	−0.03 (p=0.91)	0.09 (p=0.74)	0.06 (p=0.84)	0.23 (p=0.38)	−0.34 (p=0.19)
Hypoxic fraction	−0.42 (p=0.10)	−0.10 (p=0.72)	0.37 (p=0.16)	0.37 (p=0.16)	−0.30 (p=0.26)
Microvessel density	0.43 (p=0.07)	0.22 (p=0.37)	−0.29 (p=0.23)	−0.48 (p=0.04)	0.61 (p=0.01)
Relative level of (HK2)	−0.33 (p=0.32)	0.08 (p=0.82)	0.776 (p=0.01)	0.788 (p<0.01)	−0.804 (p<0.01)
Ki-67 score	−0.58 (p=0.01)	−0.20 (p=0.43)	0.62 (p=0.01)	0.72 (p<0.01)	−0.43 (p=0.09)
GLUT1 score	0.69 (p<0.01)	0.29 (p=0.266)	−0.73 (p<0.01)	−0.76 (p<0.001)	0.42 (p=0.10)

Discussion

This study revealed significant differences in temporal ^{18}F-FDG uptake characteristics between the basal-like MAS98.12 and the luminal-like MAS98.06 human breast cancer xenografts, both with respect to the early and the late uptake phase. Significant differences in the kinetic rate parameters k_1, k_3 and v_B were also found. Furthermore, the tumor models displayed differences in morphology, microvessel density, glucose transporter expression and proliferation. It was shown that the kinetic ^{18}F-FDG PET parameters were significantly associated with the underlying histological characteristics, in particular tumor vasculature and metabolism. Dynamic ^{18}F-FDG PET may therefore provide surrogate images of tumor physiology and may thus be relevant for prognostication and treatment stratification.

The two xenografts selected for the current study represent the two main types of breast cancer [5, 13]. The luminal-like xenograft is estrogen receptor (ER) and progesterone receptor (Pg) positive, representing hormone-dependent breast cancer growth, whereas the triple-negative (ER-, Pg-, HER2-) basal-like xenograft represents a hormone-independent subtype with poor prognosis.

The temporal ^{18}F-FDG PET uptake depends on several factors. High vessel density and permeability, GLUT1 abundance and elevated HK2 activity are expected to give increased ^{18}F-FDG uptake in breast tumors [18]. Using dynamic ^{18}F-FDG PET, a positive correlation between initial ^{18}F-FDG uptake and blood flow has been shown [19]. This indicates that the initial uptake, largely explained by the k_1 parameter, may depict tumor vasculature. We found a higher initial ^{18}F-FDG uptake in basal-like MAS98.12 xenografts and higher k_1, most likely reflecting a well-developed vasculature compared to the luminal-like MAS98.06. Also, the blood volume fraction v_B was higher in MAS98.12 xenografts. Histological examination of tissue sections supported these findings, as MAS98.12 xenografts had higher MVD. It has previously been shown that MAS98.06 xenografts do not express vascular endothelial growth factor (VEGF), but MAS98.12 xenografts do [18]. VEGFs promote blood vessel growth [20] and increase the leakiness of the vessels [21].

Absence of this growth factor can result in less developed vasculature, as is seen in MAS98.06 xenografts. We found a significant correlation between the blood volume fraction v_B and MVD, but MVD and k_1 were not significantly associated with each other (although the correlation was rather high; Table 3). It is important to note that histological features assessed in a single section can be less representative for the tumor state than a whole-tumor rate constant k_1, especially when heterogeneity in a tumor is high. In this study we also used Hoechst 33342 for assessing tumor perfusion. Compared to MVD, this approach showed similar, but less significant associations with the PET-derived parameters, and is not further discussed in the current work.

A high initial ^{18}F-FDG uptake and high k_1 may also be due to elevated GLUT1 levels. Indeed, MAS98.12 xenografts showed higher k_1 and GLUT1 expression compared to MAS98.06. In line with the obtained results, dynamic contrast-enhanced magnetic resonance imaging also showed higher tumor perfusion and blood volume in MAS98.12 xenografts compared to the MAS98.06 xenografts [22], in line with the current results.

In the late phase of the PET acquisition, the ^{18}F-FDG uptake in MAS98.06 xenografts persisted, whereas uptake in MAS98.12 xenografts reached a plateau 10 min post injection. Thus, from the raw PET data, MAS98.06 appears to be more metabolically active. In line with these findings, k_3 was significantly higher for MAS98.06 than for MAS98.12 xenografts. A significant correlation between k_3 and the level of HK2 was found, suggesting that this rate constant could be a good measure for HK2 activity. Also, MR_{FDG} was significantly associated with HK2. ^{13}C High-resolution magic angle spinning magnetic resonance spectroscopy (HR MAS MRS) [23] of tissue specimens from the two xenografts has shown that MAS98.06 has a higher rate of glycolysis than MAS98.12, supporting the current PET findings.

Clinical studies have correlated histological features to ^{18}F-FDG uptake. For breast cancer, significant positive correlations between late ^{18}F-FDG uptake and Ki-67 [11] as well as MR_{FDG} and GLUT1 expression have been found [18]. We found a positive association between the Ki-67 level and k_3, in line with these earlier results. A positive

association between GLUT1 expression and k_1 was also found in the current work. Further investigations using other tumor models are needed to explore the relations between kinetic PET parameters and histology.

Utilization of a single time point data acquisition, like SUV in conventional static PET, may not be representative for metabolic status of the tumor. As was shown in the current study, MAS98.06 had a higher ^{18}F-FDG uptake 45 min post injection compared to MAS98.12, suggesting that the former presents a more metabolically active phenotype. However, the difference in late ^{18}F-FDG uptake was not highly pronounced (25 % only), while tumor SUVs in clinical studies may show an inter-patient variability of more than 50 % [11]. On the other hand, the kinetic analysis in the current work revealed a more detailed description of tumor physiology, with larger differences between the two xenografts for some of the kinetic parameters. The kinetic parameters could be of importance in clinical studies addressing tumor aggressiveness and treatment response evaluation [11].

In conclusion, dynamic ^{18}F-FDG PET has been shown to provide in vivo depiction of tumor physiology that cannot be obtained by conventional static PET. Such measurements could be of importance in prognostication of breast cancer patients as well as treatment response evaluation, in particular when using novel therapies targeting glucose metabolism and/or formation of new vasculature.

Conflict of Interest Statement Authors declare that they have no conflict of interests

References

1. Tredan O et al. Drug resistance and the solid tumor microenvironment. Journal of the National Cancer Institute. 2007;99(19):1441–54.
2. Vaupel P, Hockel M. Blood supply, oxygenation status and metabolic micromilieu of breast cancers: characterization and therapeutic relevance. Int J Oncol. 2000;17(5):869–79.
3. Jemal A et al. Cancer statistics. CA Cancer J Clin. 2010;60(5):277–300.
4. Weigel MT, Dowsett M. Current and emerging biomarkers in breast cancer: prognosis and prediction. Endocrine-Related Cancer. 2010;17(4):R245–62.
5. Sørlie T et al. Gene expression patterns of breast carcinomas distinguish tumor subclasses with clinical implications. Proc Natl Acad Sci. 2001;98(19):10869–74.
6. Perou CM et al. Molecular portraits of human breast tumours. Nature. 2000;406(6797):747–52.
7. Sørlie T et al. Repeated observation of breast tumor subtypes in independent gene expression data sets. Proc Natl Acad Sci. 2003;100(14):8418–23.
8. Warburg O. On the origin of cancer cells. Science. 1956;123:309–14.
9. Keyes JW. SUV: Standard uptake or silly useless value? J Nucl Med. 1995;36(10):1836–9.
10. Watabe H et al. PET kinetic analysis—compartmental model. Ann Nucl Med. 2006;20(9):583–8.
11. Dunnwald LK et al. PET tumor metabolism in locally advanced breast cancer patients undergoing neoadjuvant chemotherapy: value of static versus kinetic measures of fluorodeoxyglucose uptake. Clin Cancer Res. 2011;17(8):2400–9.
12. Stasinopoulos I et al. Exploiting the tumor microenvironment for theranostic imaging. NMR Biomed. 2011;24(6):636–47.
13. Bergamaschi A et al. Molecular profiling and characterization of luminal-like and basal-like in vivo breast cancer xenograft models. Molecular Oncology. 2009;3(56):469–82.
14. Qi J, Leahy RM. Resolution and noise properties of MAP reconstruction for fully 3-D PET. IEEE Trans Med Imag. 2000;19(5):493–506.
15. Røe K et al. Preclinical dynamic 18F-FDG PET—tumor characterization and radiotherapy response assessment by kinetic compartment analysis. Acta Oncologica. 2010;49(7):914–21.
16. Kamasak ME et al. Reconstruction of kinetic parameter images directly from dynamic PET sinograms. in Medical Imaging 2005: Image Processing. San Diego: SPIE; 2005.
17. Raleigh JA et al. Relationship of hypoxia to metallothionein expression in murine tumors. Int J Radiat Oncol Biol Phys. 1998;42(4):727–30.
18. Bos R et al. Biologic correlates of 18-fluorodeoxyglucose uptake in human breast cancer measured by positron emission tomography. J Clin Oncol. 2002;20(2):379–87.
19. Tseng J et al. 18F-FDG kinetics in locally advanced breast cancer: correlation with tumor blood flow and changes in response to neoadjuvant chemotherapy. J Nucl Med. 2004;45(11):1829–37.
20. Peters KG, de Vries C, Williams LT. Vascular endothelial growth factor receptor expression during embryogenesis and tissue repair suggests a role in endothelial differentiation and blood vessel growth. Proc Natl Acad Sci USA. 1993;90(19):8915–9.
21. Collins PD, Connolly DT, Williams TJ. Characterization of the increase in vascular permeability induced by vascular permeability factor in vivo. Br J Pharmacol. 1993;109(1):195–9.
22. Huuse EM et al. In vivo MRI and histopathological assessment of tumor microenvironment in luminal-like and basal-like breast cancer xenografts. J Magn Reson Imaging. 2012;35(5):1098–107.
23. Grinde MT et al. 13C High-resolution-magic angle spinning MRS reveals differences in glucose metabolism between two breast cancer xenograft models with different gene expression patterns. NMR Biomed. 2011;24(10):1243–52.